European Journal of Neuroscience, Vol. 24, pp. 901–916, 2006 doi:10.1111/j.1460-9568.2006.04940.x

Decision-making and Weber's law: a neurophysiological model

Gustavo Deco[1] and Edmund T. Rolls[2]
[1]Institucio Catalana de Recerca i Estudis Avancats (ICREA), Universitat Pompeu Fabra, Department of Technology, Computational Neuroscience, Passeig de Circumvalacio, Barcelona, Spain
[2]University of Oxford, Department of Experimental Psychology, South Parks Road, Oxford OX1 3UD, England

Keywords: attractor networks, decision-making, integrate-and-fire neurons, multistability, spiking dynamics, Weber's law

Abstract

We describe an integrate-and-fire attractor model of the decision-related activity of ventral premotor cortex (VPC) neurons during a vibrotactile frequency comparison task [Romo *et al*. (2004) *Neuron*, 41, 165–173]. Populations of neurons for each decision in a biased competition attractor network receive a bias input that depends on the firing rates of VPC neurons that code for the two vibrotactile frequencies. The firing rate of the neurons in whichever attractor wins, reflects the sign of the difference in the frequencies (Δf) being compared but not the absolute frequencies. However, the transition from the initial spontaneous firing state to one of the two possible attractor states depends probabilistically on the difference of the vibrotactile frequencies scaled by the base frequency. This is due to finite size noise effects related to the spiking activity in the network, and the divisive feedback inhibition implemented through inhibitory interneurons. Thus the neurophysiological basis for a psychophysical effect, Weber's Law, can be related to statistical fluctuations and divisive inhibition in an attractor decision-making network.

Introduction

The link between perception and action can be conceptualized by a chain of neural operations, which leads a stimulus to guide behaviour to make a decision in favour of a particular action or motor response. For example, when subjects discriminate two stimuli separated by a time interval, the chain of neural operations encompasses mechanisms from the encoding of sensory stimuli, the attentional filtering of relevant features, their maintenance in working memory, to the crucial comparison step in the decision-making process leading to a motor response (Romo & Salinas, 2001, 2003). An important finding is that cortical areas involved in generating motor responses also show activity reflecting a gradual accumulation of evidence for choosing one or another decision, such that the process of making a decision and action generation can not be differentiated (see for example, Gold & Shadlen, 2000; Romo *et al*., 2004).

The comparison of two stimuli to judge which is the more intense becomes more difficult as they become more similar. The 'difference-threshold' is the amount of change needed for us to recognize that a change has occurred. Weber's Law (enunciated by Ernst Heinrich Weber, 1795–1878) states that the ratio of the difference-threshold to the background intensity is a constant. Theoretical models of decision-making with biologically realistic neural circuits (Wang, 2002; Machens *et al*., 2005) involve two populations of excitatory neurons engaged in competitive interactions mediated by inhibition, and external sensory inputs that bias this competition in favour of one of the populations, producing a binary choice that develops gradually. However, Weber's law has not been investigated with these models, and therefore a thorough understanding of the neural substrate underlying the comparison process and of an important psychophysical law is still missing.

We analyse the neurodynamical mechanisms engaged in the process of comparison in a decision-making paradigm from the perspective of Weber's law, that is, we investigate the probabilistic behaviour of the neural responses responsible for detecting a just-noticeable stimulus difference. We develop this theory in the context of neuronal data obtained from the ventral premotor cortex (VPC) and related areas (Romo *et al*., 2004; de Lafuente & Romo, 2005) in a vibrotactile sequential discrimination task in which subjects must decide which of two mechanical vibrations applied sequentially to their fingertips has the higher frequency of vibration (Romo & Salinas, 2003). We note that Weber's law applies to this vibrotactile task in humans and monkeys over a wide range of frequencies (Mountcastle *et al*., 1990). We model the activity of these VPC neurons by means of a theoretical framework proposed by Wang (2002), and in addition we extend the analysis to the role of finite-size fluctuations in the probabilistic behaviour of the decision-making neurodynamics, and especially the neural encoding of Weber's law. The neurodynamical formulation is based on the principle of biased competition/cooperation that has been able to simulate and explain, in a unifying framework, attention, working memory, and reward processing (Corchs & Deco, 2002; Deco & Lee, 2002; Deco & Rolls, 2002; Deco *et al*., 2002; Rolls & Deco, 2002; Deco & Rolls, 2003; Corchs & Deco, 2004; Deco & Rolls, 2004; Deco *et al*., 2004; Szabo *et al*., 2004; Deco & Rolls, 2005b).

Materials and methods

The neuronal data underlying the vibrotactile discrimination to be modelled

The neuronal substrate with the ability to discriminate two sequential vibrotactile stimuli has been investigated by Romo and colleagues

Correspondence: Professor Edmund T Rolls, as above.
E-mail: Edmund.Rolls@psy.ox.ac.uk

Received 10 February 2006, revised 19 April 2006, accepted 17 May 2006

(Romo & Salinas, 2001; Hernandez *et al*., 2002; Romo *et al*., 2002; Romo & Salinas, 2003; Romo *et al*., 2003; Romo *et al*., 2004; de Lafuente & Romo, 2005). They used a task where trained macaques (*Macaca mulatta*), must decide and report which of two mechanical vibrations applied sequentially to their fingertips has the higher frequency of vibration by pressing one of two pushbuttons. This decision-making paradigm requires therefore the following processes: (i) the perception of the first stimulus, a 500-ms long vibration at frequency f_1; (ii) the storing of a trace of the f_1 stimulus in short-term memory during a delay of typically 3 s; (iii) the perception of the second stimulus, a 500-ms long vibration at frequency f_2, and (iv) the comparison of the second stimulus f_2 to the trace of f_1, and choosing a motor act based on this comparison ($f_2 - f_1$). The vibrotactile stimuli f_1 and f_2 utilized were in the range of frequencies called flutter, i.e. within approximately 5–50 Hz. In this paper, we are particularly interested in the behaviour of VPC neurons (Romo *et al*., 2004). The activity of VPC neurons reflects the current and the remembered sensory stimuli, their comparison, and the motor response, i.e. the entire cascade of decision-making processing linking the sensory evaluation to the motor response. Many VPC neurons encode f_1 during both the stimulus presentation and the delay period. During the comparison period, the averaged firing rate of VPC neurons after a latency of a few hundred milliseconds reflects the result of the comparison, i.e. the sign of ($f_2 - f_1$), and correlates with the behavioural response of the monkey. In particular, we are interested in VPC neurons that show the strongest response only during the comparison period and reflect the sign of the comparison $f_2 - f_1$, i.e. these neurons are only activated during the presentation of f_2, with some responding to the condition $f_1 < f_2$, and others to the condition $f_1 > f_2$. These neurons, which are shown in Fig. 2G–I of Romo *et al*. (2004), reflect the decision-making step of the comparison, and therefore we will model here their probabilistic dynamical behaviour as reported by the experimental work; and through the theoretical analyses we will relate their behaviour to Weber's law.

Earlier brain areas provide inputs useful to the VPC. In the primary somatosensory area, S1, the average firing rates of neurons in S1 convey information about the vibrotactile frequency f_1 or f_2 during the stimulation period (de Lafuente & Romo, 2005). (The neuronal responses stop reflecting information about the stimuli immediately after the end of the stimulus.) The firing rates increase monotonically with stimulus frequency (Romo & Salinas, 2003). Neurons in the secondary somatosensory area, S2, respond to f_1 and show significant delay activity for a few hundred milliseconds after the end of the f_1 stimulus (Romo *et al*., 2002). Some neurons have positive and others negative monotonic relationships between their firing rate and the vibrotactile stimulus frequency. During the initial part of f_2 (~200 ms) the firing rate reflects either f_1 or f_2; later, during the last 300 ms, the firing rate reflects the comparison ($f_2 - f_1$), and therefore the result of the decision. Prefrontal cortex (PFC) neurons (Brody *et al*., 2003a) also have a positive or negative monotonic firing rate relationship with f_1. Furthermore, PFC neurons convey information about f_1 through the delay period so that information about f_1 is present when f_2 arrives. Medial premotor cortex (MPC) neurons respond during f_1 itself, with either positive or negative monotonic firing rate relationships, during the late part of the delay period in an f_1-dependent manner, and during the comparison period reflecting the comparison $f_2 - f_1$ (Hernandez *et al*., 2002).

In summary, in the sequential vibrotactile discrimination task, S1 is predominantly sensory and the primary motor cortex (M1) is predominantly motor. A number of other cortical areas have activity that reflects the encoding, short-term memory, and comparison functions involved, perhaps as a result of information exchange between these cortical areas; the differences between S2, MPC and VPC are reflected mainly in their different latencies (R. Romo, personal communication). In a detection task, the activity of S1 neurons codes for the stimulus but not for the behavioural choice made, whereas neuronal activity in MPC correlates with behavioural choice and detection (de Lafuente & Romo, 2005). Within this context, VPC (and MPC) neurons seem to reflect the core of the processing that links sensory information with action, and therefore they may represent the decision-making process itself, rather than the representation of the stimulus. Consequently, VPC neurons are excellent candidates for encoding also the probabilistic behavioural response as expressed in Weber's law. Key questions are, how VPC neurons (or neurons with similar activity in connected areas such as MPC) implement the decision-making process? What are the principles by which the probabilistic decisions are taken? How is the processing implemented by the neurons?

Theoretical framework: a probabilistic attractor network

The theoretical framework within which the new model was developed was utilized by Wang (2002), which is based on a neurodynamical model first introduced by Brunel & Wang (2001), and which has been recently extended and successfully applied to explain several experimental paradigms (Deco & Rolls, 2002; Rolls & Deco, 2002; Deco & Rolls, 2003; Deco *et al*., 2004; Szabo *et al*., 2004; Deco & Rolls, 2005b; Deco *et al*., 2005).

In this framework, we model probabilistic decision-making by a network of interacting neurons organized into a discrete set of populations, as depicted in Fig. 1. Populations or pools of neurons are defined as groups of excitatory or inhibitory neurons sharing the same inputs and connectivities. The network contains N_E (excitatory) pyramidal cells and N_I inhibitory interneurons. In our simulations, we use $N_E = 800$ and $N_I = 200$, consistent with the neurophysiologically observed proportion of 80% pyramidal cells vs. 20% interneurons (Abeles, 1991; Rolls & Deco, 2002). The neurons are fully connected (with synaptic strengths as specified below). The specific populations have specific functions in the task. In our minimal model, we assume that the specific populations encode the categorical result of the comparison between the two sequentially applied vibrotactile stimulation, f_1 and f_2, i.e. the result that $f_1 > f_2$ or the result that $f_1 < f_2$. Each specific population of excitatory cells contains rN_E neurons (in our simulations $r = 0.1$). In addition there is one non-specific population, named 'Non-specific', which groups all other excitatory neurons in the modelled brain area not involved in the present tasks, and one inhibitory population, named 'Inhibitory', grouping the local inhibitory neurons in the modelled brain area. The latter population regulates the overall activity and implements competition in the network by spreading a global inhibition signal.

Because we are mainly interested in the non-stationary probabilistic behaviour of the network, the proper level of description at the microscopic level is captured by the spiking and synaptic dynamics of one-compartment integrate-and-fire (IF) neuron models (Deco & Rolls, 2005a). An IF neuron integrates the afferent current generated by the incoming spikes, and fires when the depolarization of the cell membrane crosses a threshold. At this level of detail the model allows the use of realistic biophysical time constants, latencies and conductances to model the synaptic current, which in turn allows a thorough study of the realistic time scales and firing rates involved in the time evolution of the neural activity. Consequently, the simulated neuronal dynamics, that putatively underlie cognitive processes, can be quantitatively compared with experimental data. For this reason, it

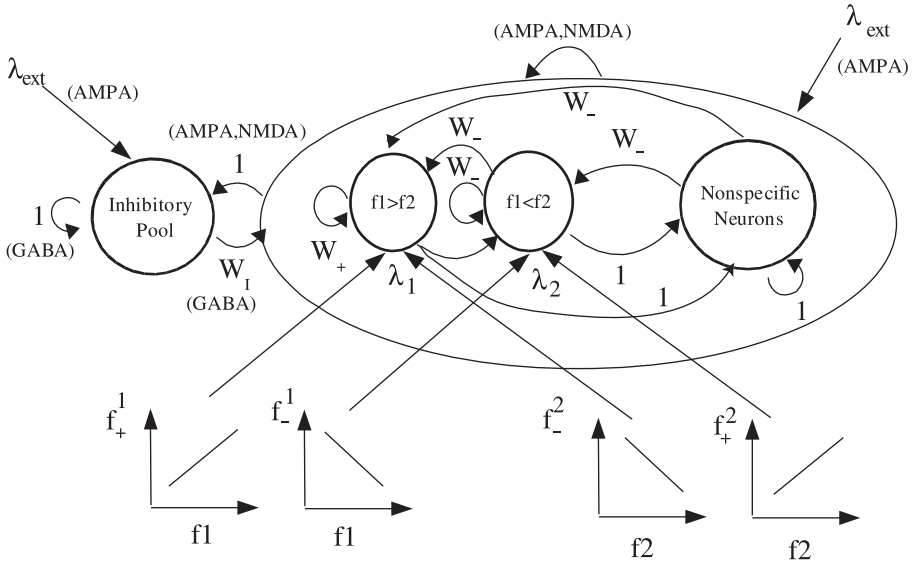

FIG. 1. The architecture of the neurodynamical model for a probabilistic decision-making network. The single attractor network has two populations or pools of neurons ($f_1 > f_2$) and ($f_1 < f_2$) which represent the decision states. One of these pools becomes active when a decision is made. If pool ($f_1 > f_2$) is active, this corresponds to the decision that stimulus f_1 is greater than stimulus f_2. There is also a population of non-specific excitatory neurons, and a population of inhibitory neurons. Pool ($f_1 > f_2$) is biased by λ_1, which reflects the strength of stimulus f_1, and pool ($f_2 > f_1$) is biased by λ_2, which reflects the strength of stimulus f_2. (In the simulations performed f_1 is the frequency of vibrotactile stimulus 1, f_2 is the frequency of vibrotactile stimulus 2, and the stimuli must be compared to decide which is of the higher frequency. The bias input to pool ($f_1 > f_2$) is $\lambda_1 = f_+^1 + f_-^2$, and to pool ($f_1 < f_2$) is $\lambda_2 = f_-^1 + f_+^2$, where f_+^1 is the firing rate of the neurons recorded neurophysiologically that respond to f_1 with a monotonically increasing rate, and f_-^2 is the firing rate of the neurons that respond to f_2 with a monotonically decreasing rate.) The integrate and fire network is subject to finite size noise, and therefore probabilistically settles into either an attractor with the population ($f_1 > f_2$) active, or with the population ($f_1 < f_2$) active, depending on the biasing inputs λ_1 and λ_2. The network is thus a biased competition model of decision-making. The weights connecting the different populations of neurons are shown as w_+, w_-, w_I, and 1, and the values found in the mean field analysis are given in the text. All neurons receive a small random Poisson set of input spikes λ_{ext} from other neurons in the system.

is very useful to include a thorough description of the different time constants of the synaptic activity. The IF neurons are modelled as having three types of receptor mediating the synaptic currents flowing into them; AMPA, NMDA (both activated by glutamate), and GABA receptors. The excitatory recurrent postsynaptic currents (EPSCs) are considered to be mediated by AMPA (fast) and NMDA (slow) receptors; external EPSCs imposed onto the network from outside are modelled as being driven only by AMPA receptors. Inhibitory postsynaptic currents (IPSCs) to both excitatory and inhibitory neurons are mediated by GABA receptors. The details of the mathematical formulation are summarized in previous papers (Brunel & Wang, 2001; Deco & Rolls, 2005b), and are provided in Appendix 1.

We modulate the conductance values for the synapses between pairs of neurons by connection weights, which can deviate from their default value, 1. The structure and function of the network are achieved by differentially setting the weights within and between populations of neurons. The labelling of the weights is defined in Fig. 1. We assume that the connections are already formed, by for example earlier self-organization mechanisms, as if they were established by Hebbian learning, i.e. the coupling will be strong if the pair of neurons have correlated activity (i.e. covarying firing rates), and weak if they are activated in an uncorrelated way. We assume that the two decisions '$f_1 > f_2$' and '$f_1 < f_2$', corresponding to the two categories, are already encoded, in the sense that the monkey is already trained that pushing one or the other button, but not both, might produce a reward. As a consequence of this, neurons within a specific excitatory population are mutually coupled with a strong weight, w_+. Furthermore, the populations encoding for these two decisions are likely to have anti-correlated activity in this behavioural context, resulting in weaker than average connections between the two different populations. Consequently, we choose a weaker value $w_- = 1 - r(w_+ - 1)/(1 - r)$, so that the overall recurrent excitatory synaptic drive in the spontaneous state remains constant as w_+ is varied (Brunel & Wang, 2001). Neurons in the inhibitory population are mutually connected with an intermediate weight $w = 1$. They are also connected with all excitatory neurons in the same layer with the same intermediate weight, which for excitatory-to-inhibitory connections is $w = 1$, and for inhibitory-to-excitatory connections is denoted by a weight w_I. Neurons in a specific excitatory population are connected to neurons in the non-selective population in the same layer with a feedforward synaptic weight $w = 1$ and a feedback synaptic connection of weight w_-.

Each individual population is driven by two different kinds of input. First, all neurons in the model network receive spontaneous background activity from outside the module through $N_{ext} = 800$ external excitatory connections. Each connection carries a Poisson spike train at a spontaneous rate of 3 Hz, which is a typical spontaneous firing rate value observed in the cerebral cortex. This results in a background external input with a rate of 2.4 kHz for each neuron. Second, the neurons in the two specific populations additionally receive external inputs encoding stimulus-specific information. They are assumed to originate from the somatosensory area S2 and from the PFC, encoding the frequency of both stimuli f_1 (stored) and f_2 (present) to be compared during the comparison period, i.e. when the second stimulus is applied. As described above, there are two types of S2 and PFC neurons, namely, neurons with positive and others with negative monotonic relationships between the firing rate and the stimulus vibrotactile frequency. Based on the experimental results (Brody *et al*., 2002; Romo *et al*., 2004), we model the firing rate of

positive monotonic neurons by $f_+^x = 5\text{Hz} + 2.3f_x$, and the firing rate of negative monotonic neurons by $f_-^x = 25\text{Hz} - 0.6f_x$, where f_x is the 25Hz - 0.6 frequency of the vibrotactile stimulation in Hz (i.e. f_x is equal to f_1 or f_2). When stimulating, the rate of the Poisson train to the neurons of the specific population ($f_1 > f_2$) is increased by an extra value of $\lambda_1 = f_+^1 + f_-^2$, and to population ($f_1 < f_2$) by $\lambda_2 = f_-^1 + f_+^2$, as these encode the two vibrotactile stimuli to be compared. Although in the neurophysiological experiments of Romo *et al*. (2004) there was a delay between the application of f_1 and f_2, we assume that information about f_1 is maintained through the delay period by the activity of neurons in the prefrontal cortex as described above using short-term attractor memory dynamics, as has been previously modelled (Brody *et al*., 2003b; Machens *et al*., 2005). In this paper, we focus on the probabilistic decision-making process itself and the role of statistical fluctuations in a spiking network rather than the short-term memory required to remember f_1, and how Weber's law is related to this processing. We note that the probabilistic decision-making model applies generically, and need not be implemented by neurons in VPC in particular.

Results

The model

The architecture of the neurodynamical model for a probabilistic decision-making network is as follows, with the details described in the Materials and methods. f_1 is the frequency of vibrotactile stimulus 1, f_2 is the frequency of vibrotactile stimulus 2, and the stimuli must be compared to decide which is of the higher frequency. The single attractor network has two populations or pools of neurons ($f_1 > f_2$) and ($f_1 < f_2$) which represent the decision states (see Fig. 1). One of these pools becomes active when a decision is made. If pool ($f_1 > f_2$) is active, this corresponds to the decision that stimulus f_1 is greater than stimulus f_2. There is also a population of non-specific excitatory neurons, and a population of inhibitory neurons. Pool ($f_1 > f_2$) is biased by λ_1 which reflects the frequency of stimulus f_1, and pool ($f_2 > f_1$) is biased by λ_2 which reflects the frequency of stimulus f_2. The integrate-and-fire network is subject to finite size noise, and therefore probabilistically settles into either an attractor with the population ($f_1 > f_2$) active, or with the population ($f_1 < f_2$) active, depending on the biasing inputs λ_1 and λ_2. The network is thus a biased competition model of decision-making. The weights connecting the different populations of neurons are shown as w_+, w_-, w_{I}, and 1, and the values established as a result of a mean field analysis are given in the Materials and methods. All neurons receive a small random Poisson set of input spikes λ_{ext} from other neurons in the system.

Stationary multistability analysis: mean-field

A first requirement for using the network described above and in the Materials and methods as a probabilistic decision-making neurodynamical framework is to tune its connectivity such that the network operates in a regime of multistability. This means that at least for the stationary conditions, i.e. for periods after the dynamical transients, different possible attractors are stable. The attractors of interest for our task correspond to high activation (high spiking rates) or low activation (low spiking rates) of the neurons in the specific populations ($f_1 > f_2$) and ($f_1 < f_2$). The activation of the specific population ($f_1 > f_2$) and the simultaneous lack of activation of the specific population ($f_1 < f_2$) corresponds to encoding associated with a motor response of the monkey reporting the categorical decision $f_1 > f_2$. The opposite decision corresponds to the opposite attractor states in the two specific neuronal populations. Low activity in both specific populations (the 'spontaneous state') corresponds to encoding that no decision has been made, i.e. the monkey does not answer or generates a random motor response. The same happens if both specific populations are activated (the 'pair state'). Because the monkey responds in a probabilistic way depending on the different stimuli, the operating working point of the network should be such that both possible categorical decisions, i.e. both possible single states, and sometimes (depending on the stimuli) the pair and spontaneous states, are possible stable states.

The network's operating regimes just described can all occur if the synaptic connection weights are appropriate. To determine the correct weights a mean field analysis was performed. Although a network of integrate-and-fire with randomness in the spikes being received is necessary to understand the dynamics of the network, and how these are related to probabilistic decision making, this means that the spiking activities fluctuate from time-point to time-point and from trial to trial. Consequently, integrate-and-fire simulations are computationally expensive and their results probabilistic, which makes them rather unsuitable for systematic parameter explorations. To solve this problem, we simplify the dynamics via the mean field approach at least for the stationary conditions, i.e. for periods after the dynamical transients, and then analyse the bifurcation diagrams of the dynamics. The essence of the mean-field approximation is to simplify the integrate-and-fire equations by replacing after the diffusion approximation (Tuckwell, 1988; Amit & Brunel, 1997; Brunel & Wang, 2001), the sums of the synaptic components by the average DC component and a fluctuation term. The stationary dynamics of each population can be described by the population transfer function, which provides the average population rate as a function of the average input current. The set of stationary, self-reproducing rates ν_i for the different populations i in the network can be found by solving a set of coupled self-consistency equations using the formulation derived by Brunel & Wang (2001) (see Appendix 2). The equations governing the activities in the mean-field approximation can hence be studied by standard methods of dynamical systems. The formulation departs from the equations describing the dynamics of one neuron to reach a stochastic analysis of the mean-first passage time of the membrane potentials, which results in a description of the population spiking rates as functions of the model parameters, in the limit of very large N. Obtaining a mean-field analysis of the stationary states that is consistent with the network when operating dynamically as an integrate-and-fire network is an important part of the approach we use.

To investigate how the stable states depend on the connection parameters w_+ and w_{I}, we solved the mean-field equations for particular values of these parameters starting at different initial conditions. For example, to investigate the stability of the state described by population ($f_1 > f_2$) being in an active state and all other populations inactive, we initialize the system with that population at 10 Hz, all other excitatory populations (including the non-specific ones) at 3 Hz, and the inhibitory population at 9 Hz. If and only if, after solving the equations numerically, the population ($f_1 > f_2$) is still active (meaning that they have a firing rate ≥10 Hz) but no other excitatory population is active, we conclude that the state is stable. [For all simulation periods studied, the mean-field equations were integrated using the Euler method with step size 0.1 and 4000 iterations, which always allowed for convergence.] This procedure is then repeated for all other combinations of w_+ and w_{I} to find the region where the active population ($f_1 > f_2$) is stable. The stable regions of the other states are found in the same way.

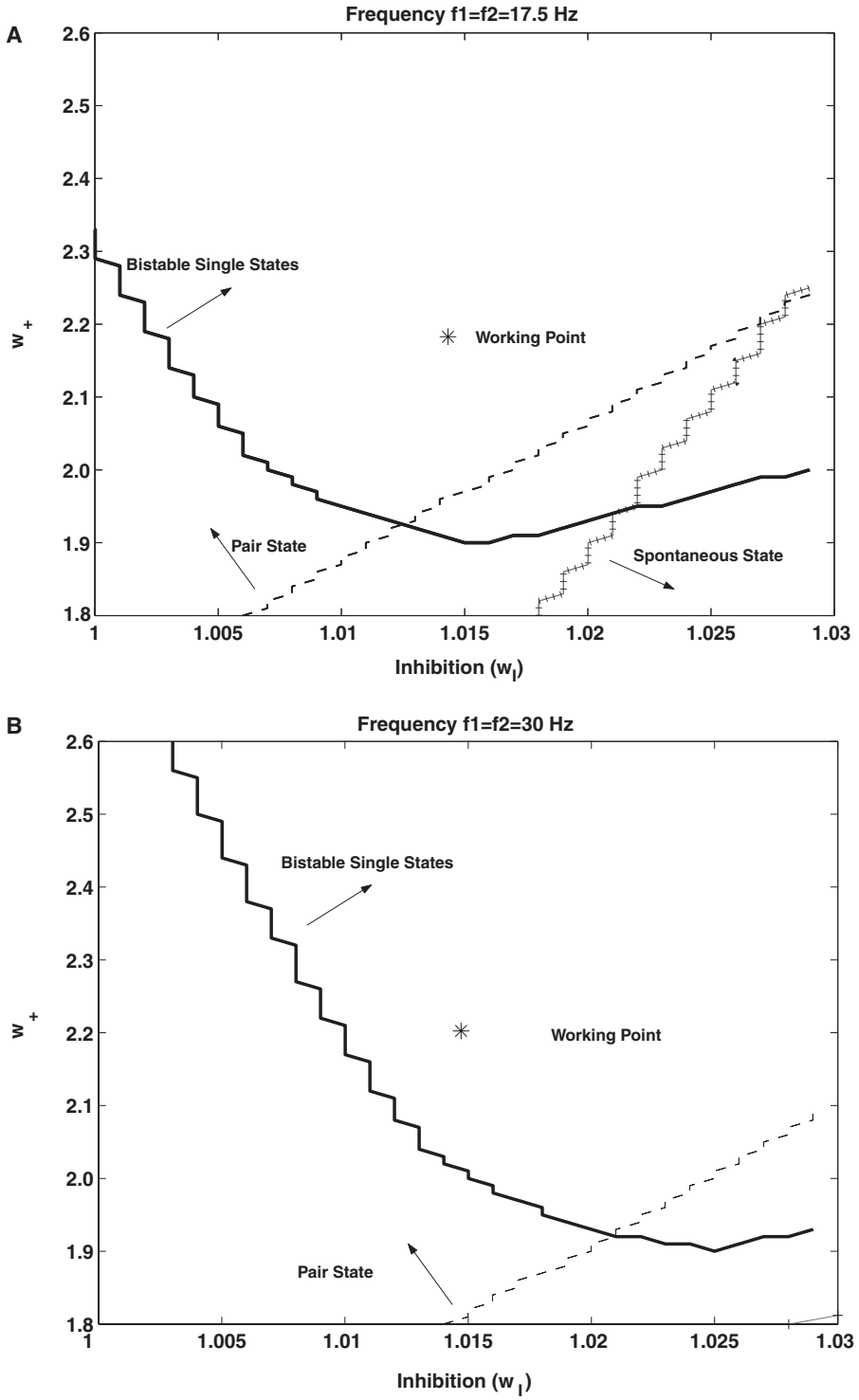

FIG. 2. Bifurcation diagrams resulting from the mean-field analysis, for a particular case where the behavioural decision-making is at chance due to f_1 and f_2 being equal. (A and B) Show how the stable states of the average firing rate vary as a function of the synaptic strengths w_+ and w_I for the extreme cases: (A) $f_1 = f_2 = 17.5$ Hz corresponding to a low frequency of vibrotactile stimulation; and (B) $f_1 = f_2 = 30$ Hz corresponding to a high frequency of vibrotactile stimulation. In these cases, the specific neuronal populations ($f_1 > f_2$) and ($f_1 < f_2$) received an extra stimulation of $\lambda_1 = f_+^1 + f_-^2$ and $\lambda_2 = f_-^1 + f_+^2$, respectively, as these encode the two vibrotactile stimuli to be compared. The different regions where single states, a pair state, and a spontaneous firing rate state are stable are shown. In the study, we focus on the region of multistability, so that a probabilistic decision is possible, and therefore a convenient working point is one corresponding to a connectivity given by $w_+ = 2.2$ and $w_I = 1.015$.

Figure 2 presents the bifurcation diagrams resulting from the mean-field analysis, for a particular case where the behavioural decision-making is hardest and is in fact purely random (i.e. at chance) due to an equality between f_1 and f_2. Figure 2A and B show how the stable states of average firing rate vary as a function of the strength of w_+ and w_I for the extreme cases: (i) $f_1 = f_2 = 17.5$ Hz corresponding to a low frequency of vibrotactile stimulation (Fig. 2A); and (ii) $f_1 = f_2 = 30$ Hz corresponding to a high frequency of stimulation

(Fig. 2B). In these cases, the specific populations ($f_1 > f_2$) and ($f_1 < f_2$) received an extra stimulation of $\lambda_1 = f_+^1 + f_-^2$; and $\lambda_2 = f_-^1 + f_+^2$, respectively, encoding the two vibrotactile stimuli to be compared. (The way in which these λ-values were calculated simply reflects the neurons recorded in the VPC and connected areas, as described in the Materials and methods.) The different regions where single states, a pair state, and a spontaneous state are stable are shown. In our study, we focus on a region of multistability, so that a probabilistic decision is possible, and therefore a convenient working point (see Fig. 2) is one corresponding to a connectivity given by $w_+ = 2.2$ and $w_I = 1.015$. We used this operating working point derived from the mean field analysis for all the integrate-and-fire simulations shown in this paper, to produce probabilistic (multistable) behaviour of the network. Overall, Fig. 2 shows very large regions of stability, so that the network behaviour described here is very robust.

Non-stationary probabilistic analysis: spiking dynamics

A full characterization of the dynamics, and especially of its probabilistic behaviour, including the non-stationary regime of the system, can only be obtained through computer simulations of the spiking network model. Moreover, these simulations enable comparisons between the model in which spikes occur and neurophysiological data. The simulations of the spiking dynamics of the network were integrated numerically using the second order Runge–Kutta method with step size 0.05 ms. Each simulation was started by a period of 500 ms where no stimulus was presented to allow the network to stabilize. The non-stationary evolution of spiking activity was averaged over 200 trials initialized with different random seeds. In all cases, we aimed to model the behaviour of the VPC neurons as shown in Fig. 2G–I of Romo *et al*. (2004) which reflect the decision-making performed during the comparison period. Therefore, we study the non-stationary probabilistic behaviour of the spiking network defined in Fig. 1, during this comparison period (during the presentation of f_2), by stimulating the network simultaneously with f_1 and f_2. This is carried out by increasing the rate of the Poisson train to the neurons of both specific populations ($f_1 > f_2$) and ($f_1 < f_2$) by an extra value of $\lambda_1 = f_+^1 + f_-^2$ and $\lambda_2 = f_-^1 + f_+^2$, respectively, as these encode the two vibrotactile stimuli to be compared (see Materials and methods).

Figure 3 shows the probability of correct discrimination as a function of the difference between the two presented vibrotactile frequencies to be compared. We assume that $f_1 > f_2$ by a Δ-value, i.e. $f_1 = f_2 + \Delta$. [In Fig. 3 this value is called 'Delta frequency ($f_1 - f_2$)']. Each diamond-point in the figure corresponds to the result calculated by averaging 200 trials of the full-spiking simulations. The lines were calculated by fitting the points with a logarithmic function. A correct classification occurs when during the 500-ms comparison period, the network evolves to a 'single-state' attractor that shows a high level of spiking activity (larger than 10 Hz) for the population ($f_1 > f_2$), and simultaneously a low level of spiking activity for the population ($f_1 < f_2$) (at the level of the spontaneous activity). One can observe from the different panels corresponding to different base vibrotactile frequencies f_2, that reaching a threshold of correct classification of, for example 85% (horizontal dashed line in Fig. 3), the difference between f_1 and f_2 must become larger as f_2 increases. We show in the second panel of Fig. 3 a good fit between the actual neuronal data described by Romo & Salinas (2003) for the $f_2 = 20$ Hz condition (indicated by *), and the results obtained with the model. Figure 4 plots the critical discrimination Δ-value corresponding to an 85% correct performance level (the 'difference-threshold') as a function of the base-frequency

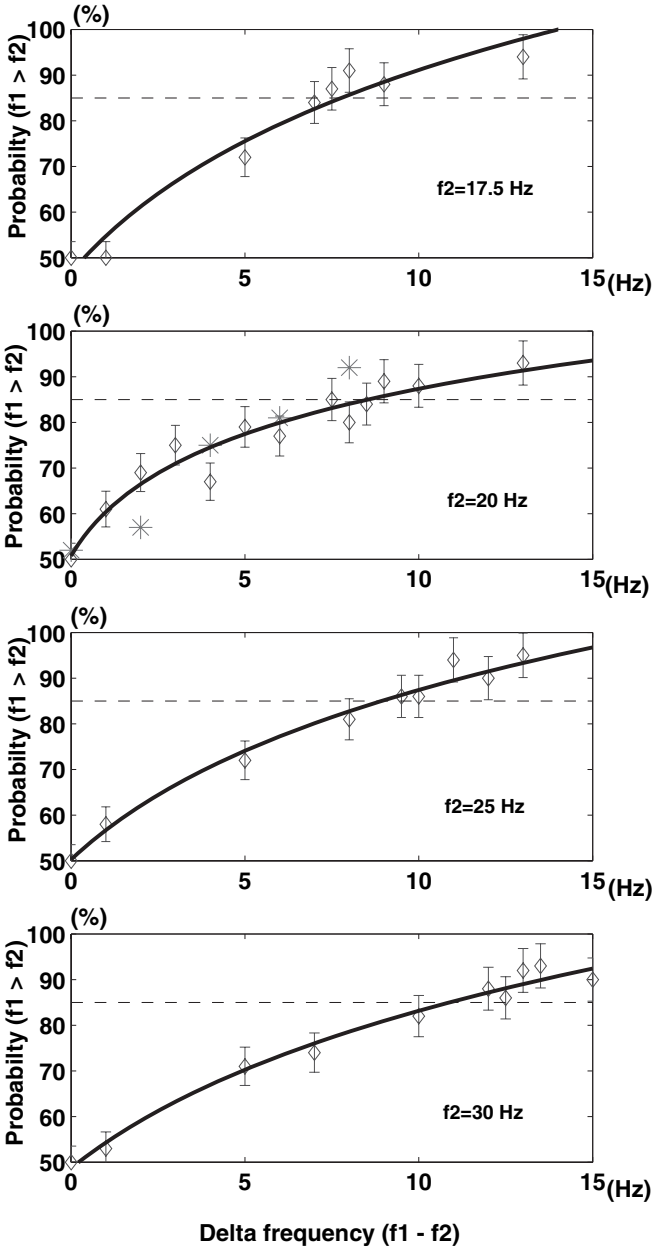

FIG. 3. Probability of correct discrimination as a function of the difference between the two presented vibrotactile frequencies to be compared. In the simulations, we assume that $f_1 > f_2$ by a Δ-value (labelled 'Delta frequency ($f_1 - f_2$)', i.e. $f_1 = f_2 + \Delta$. The points correspond to the trial averaged spiking simulations. The line interpolates the points with a logarithmic function. The horizontal dashed line represents the threshold of correct classification for a performance of 85% correct discrimination. The error bars in this and the other figures show the standard deviation of the sampled mean. The second panel down includes actual neuronal data described by Romo & Salinas (2003) for the $f_2 = 20$ Hz condition (indicated by *).

f_2. The 'difference-threshold' increases linearly as a function of the base-frequency. This corresponds to Weber's law for the vibrotactile discrimination task.

The analysis shown in Figs 3 and 4 suggests that Weber's law, and consequently the ability to discriminate two stimuli, is encoded in the probability of performing a transition to the correct final attractor. To reinforce this hypothesis, we show in Fig. 5 that Weber's law is not encoded in the firing rate of the VPC decision-making neurons that we are modelling. We simulate again a situation corresponding to the

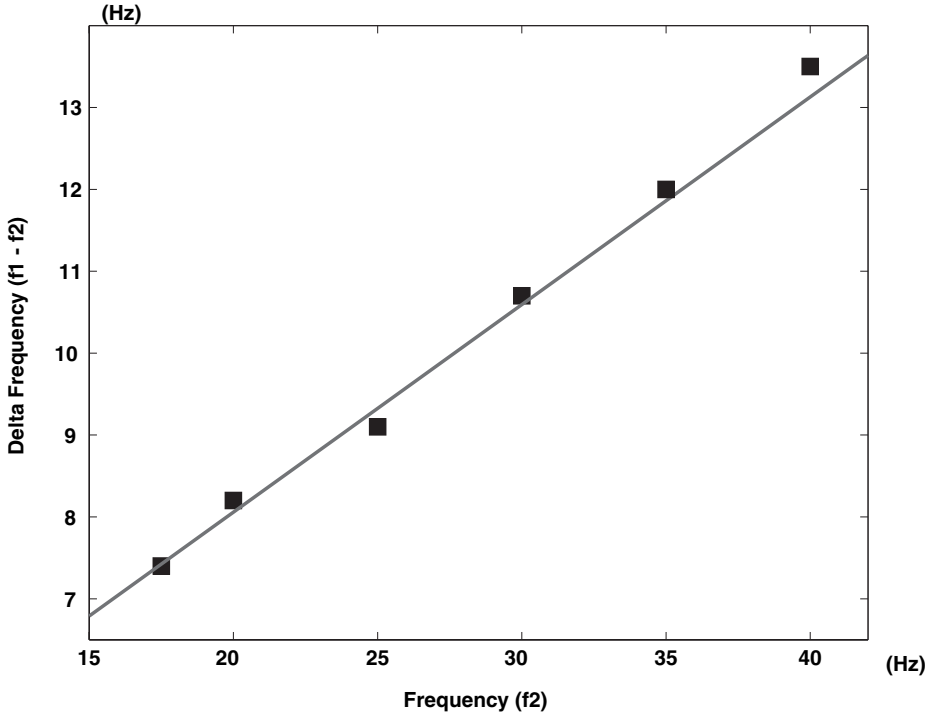

FIG. 4. Weber's law for the vibrotactile discrimination task. The critical discrimination Δ-value ('difference-threshold') is shown corresponding to an 85% correct performance level as a function of the base frequency f_2. The 'difference-threshold' increases linearly as a function of the base frequency.

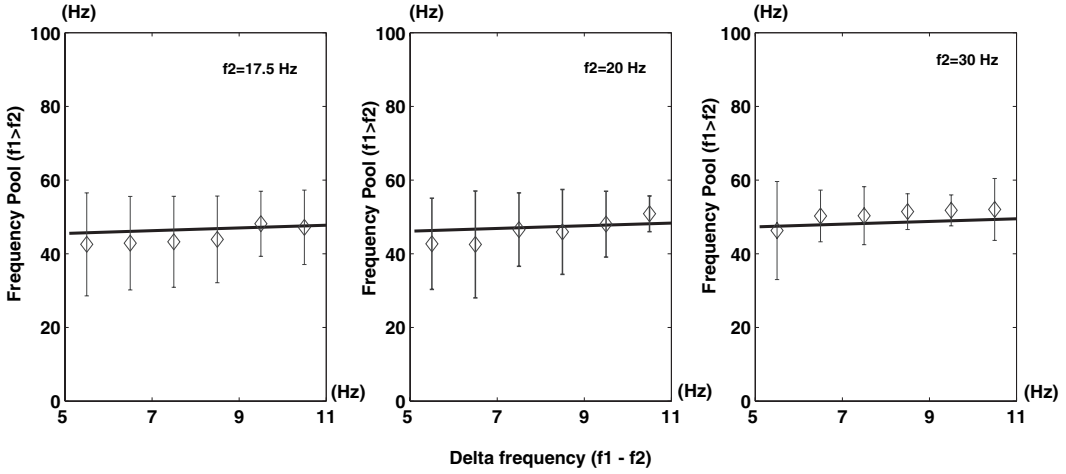

FIG. 5. Final stationary spiking rate of the ($f_1 < f_2$) population (after transients) as a function of the difference between the two vibrotactile frequencies to be compared, for the cases where this population correctly won the competition and the network has performed a transition to the proper attractor. The plots shows the results obtained with the spiking simulations (diamond-points correspond to the average values over 200 trials, and the error bars to the standard deviation). The lines correspond to the mean-field calculations. The rate of the population encoding the result of the comparison is independent of f_2 and of the difference between f_1 and f_2.

cases where f_1 is larger than f_2 by a Δ-value, and therefore the network will perform correctly when the dynamics perform a transition to the final single attractor corresponding to high activity in the population ($f_1 > f_2$) and low activity in the population ($f_1 < f_2$). Figure 5 plots for three different frequencies f_2, the rate of the ($f_1 < f_2$) population (for the cases where this population correctly won the competition and the network has performed a transition to the proper attractor) as a function of the difference between the two vibrotactile frequencies to be compared. The plots show the results obtained with the spiking simulations (the diamond-points correspond to the average values over 200 trials, and the error bars to the standard deviation). The lines correspond to the mean-field calculations. A good agreement between the spiking simulations and the consistent mean-field results is observed. The most interesting observation is the fact that the firing rate of the population ($f_1 > f_2$) in the correct attractor, for different base frequencies f_2 and for different differences between f_1 and f_2 (Δf), is practically constant, i.e. the firing rate of the population encoding the result of the comparison does not encode Weber's law. The decision making process that gives rise to Weber's law is thus represented in the dynamics of which attractor/decision state is reached probabilistically, and not on the final firing rates of the neurons in the attractor/decision state.

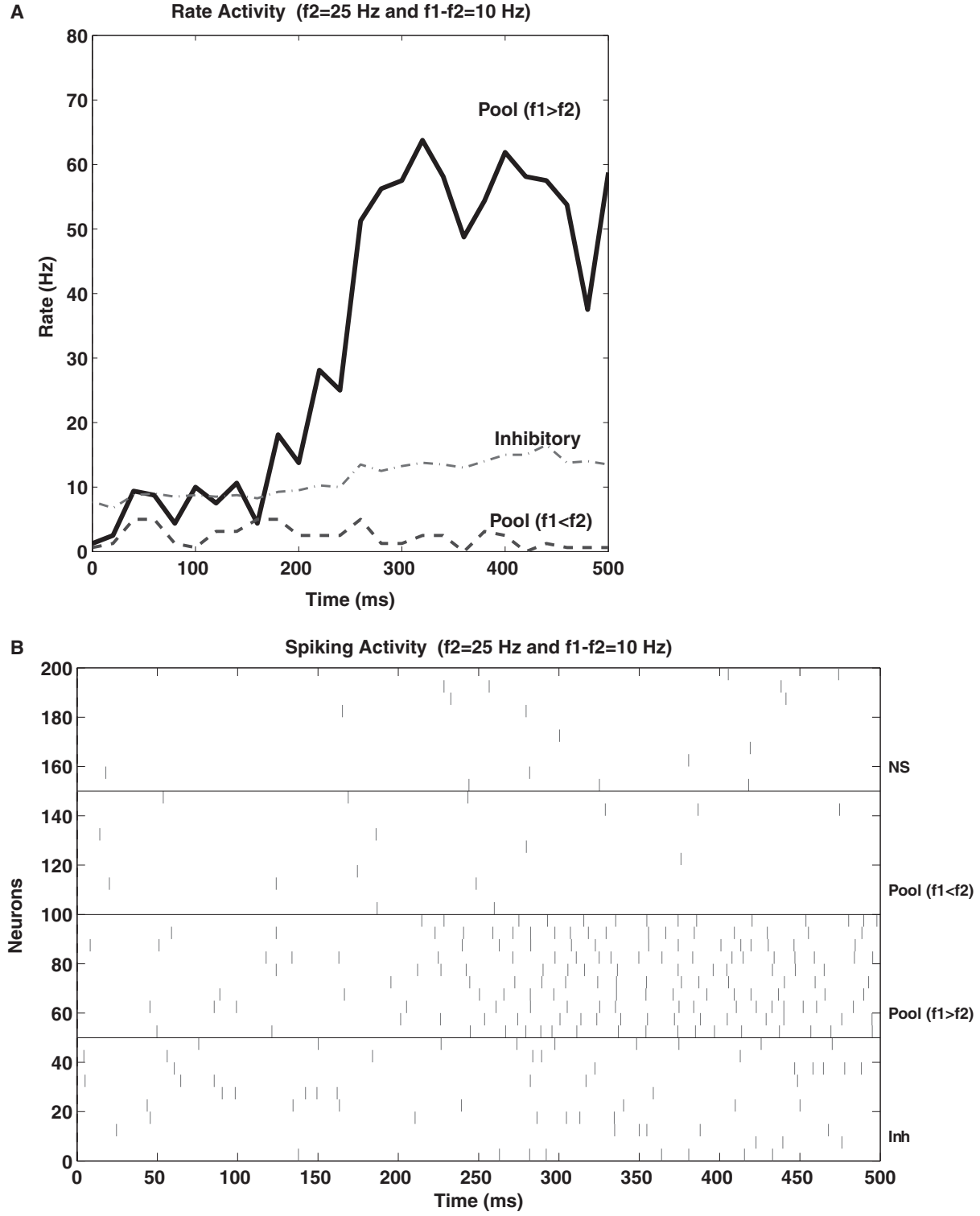

FIG. 6. Dynamical evolution of the network activity of VPC neurons during the comparison period for the specific case of having $f_1 = 30$ Hz and $f_2 = 20$ Hz. (A) plots the evolution of the spiking rate of the populations ($f_1 > f_2$) ($f_1 < f_2$) and the inhibitory population as a function of time. The utilized bin widths for the simulations were 20 ms. (B) plots the corresponding rastergrams of ten randomly selected neurons for each pool in the network. Each vertical line corresponds to the generation of a spike. The spatio-temporal spiking activity shows the transition to the correct final single-state attractor, i.e. a transition to the correct final attractor encoding the result of the discrimination ($f_1 > f_2$). We observe that after 200 ms the populations ($f_1 > f_2$) and ($f_1 < f_2$) start to separate, in such a way that the population ($f_1 > f_2$) wins the competition and the network performs a transition to a single-state final attractor corresponding to a correct discrimination [i.e. high activity in the population ($f_1 > f_2$) and low activity in the population ($f_1 < f_2$)].

Figure 6 shows a typical evolution of the network of VPC neurons during the comparison period for the specific case of having $f_1 = 30$ Hz and $f_2 = 20$ Hz. The top part of Fig. 6 plots the evolution of the spiking rate of the populations ($f_1 > f_2$) ($f_1 < f_2$), and the inhibitory population as a function of time. The utilized bin widths for the simulations were 20 ms. The transition shown corresponds to a

correct trial, i.e. showing a transition to the correct final attractor encoding the result of the discrimination $f_1 > f_2$. We observe that after 200 ms the populations ($f_1 > f_2$) and ($f_1 < f_2$) start to separate in such a way that the population ($f_1 > f_2$) wins the competition and the network performs a transition to a single-state final attractor corresponding to a correct discrimination [i.e. high activity in the population ($f_1 > f_2$) and low activity in the population ($f_1 < f_2$)]. The bottom part of Fig. 6 plots the corresponding rastergrams of ten randomly selected neurons for each pool in the network. Each vertical line corresponds to the generation of a spike. The spatio-temporal spiking activity shows the transition to the correct final single-state attractor.

In Fig. 2G–I of Romo *et al*. (2004), the authors analysed the response during f_2 of single VPC neurons performing the comparison as a function of both f_1 and f_2. Figure 7 shows the numerical results and analysis corresponding to those cases. Figure 7A plots a neuron of the population ($f_1 < f_2$) during the comparison period of f_1 and f_2 vibrotactile stimulation. The labels on the left indicate f_1, f_2 pairs in terms of the vibrotactile frequencies. Each row of ticks is a trial, and each tick is a spike. All neurons were tested with ten trials per stimulus pair, selecting only trials where the network performed correctly. The top five cases correspond to a situation where $f_1 < f_2$ and therefore the population ($f_1 < f_2$) is highly activated after 100–200 ms. The following five cases at the bottom correspond to a situation where $f_1 > f_2$ and therefore the population ($f_1 < f_2$) is not activated. (The population ($f_1 > f_2$), not shown in Fig. 7, won the competition in the five cases shown at the bottom of Fig. 7A, and therefore inhibited the ($f_1 < f_2$) population in the correctly discriminated trials selected for this figure). Figure 7B plots the average firing rate as a function of f_1 and f_2. The plots show the results obtained with the spiking simulations (diamond-points correspond to the average values over 200 trials, and the error bars to the standard deviation). The lines correspond to the mean-field calculations. The black indicates $f_1 < f_2$ ($f_2 = f_1 + 8$ Hz) and grey $f_1 > f_2$ ($f_2 = f_1 - 8$ Hz). The average firing rate of the population ($f_1 < f_2$) is only dependent on the sign of $f_2 - f_1$ and is not dependent on f_1, f_2, or on the absolute value of the difference $|f_1 - f_2|$, confirming again (also as in the neurophysiological experiments) that Weber's Law can not be encoded in the firing rate, but only in the probability with which that firing rate can be reached (which is dependent on the sign and magnitude of the difference between f_1 and f_2).

To analyse more quantitatively the dependence of the average firing rate of the VPC neurons encoding the comparisons as a function of f_1 and f_2, Romo *et al*. (2004) fitted and plotted the time evolution of the coefficients that directly measure the dependence on f_1 and f_2. Let us denote by $r(t)$ the trial averaged firing rate of the population ($f_1 < f_2$) at time t. We determined the coefficients $a_1(t)$, $a_2(t)$ and $a_3(t)$ that fit the firing rate of the population ($f_1 < f_2$) according to $r(t) = a_1(t)f_1 + a_2(t)f_2 + a_3(t)f_3$. We considered for all ten f_1,f_2 pair combinations shown in Fig. 7A, 50 correct trials, using a bin width of 50 ms. Figure 7C plots the evolution of $a_1(t)$ and $a_2(t)$ during the comparison period. In this figure, both coefficients evolve in an antisymmetrical fashion, indicating that the average firing rate $r(t)$ depends only on the difference between f_1 and f_2 [i.e. $a_1(t) = -a_2(t)$]. Even more, in the range of vibrotactile flutter frequencies, the simulation and neurophysiological results show that the firing rate depends significantly only on the sign of the difference and not on the magnitudes of the vibrotactile frequency values.

Thus the present theoretical analysis suggests a specific neurophysiological prediction, that Weber's Law for frequency discrimination could be implemented not by the firing rate of a given population of neurons (which reflects just the sign of the difference between f_1 and f_2), but by the probability that that particular population will be activated, which is influenced by both the difference between f_1 and f_2

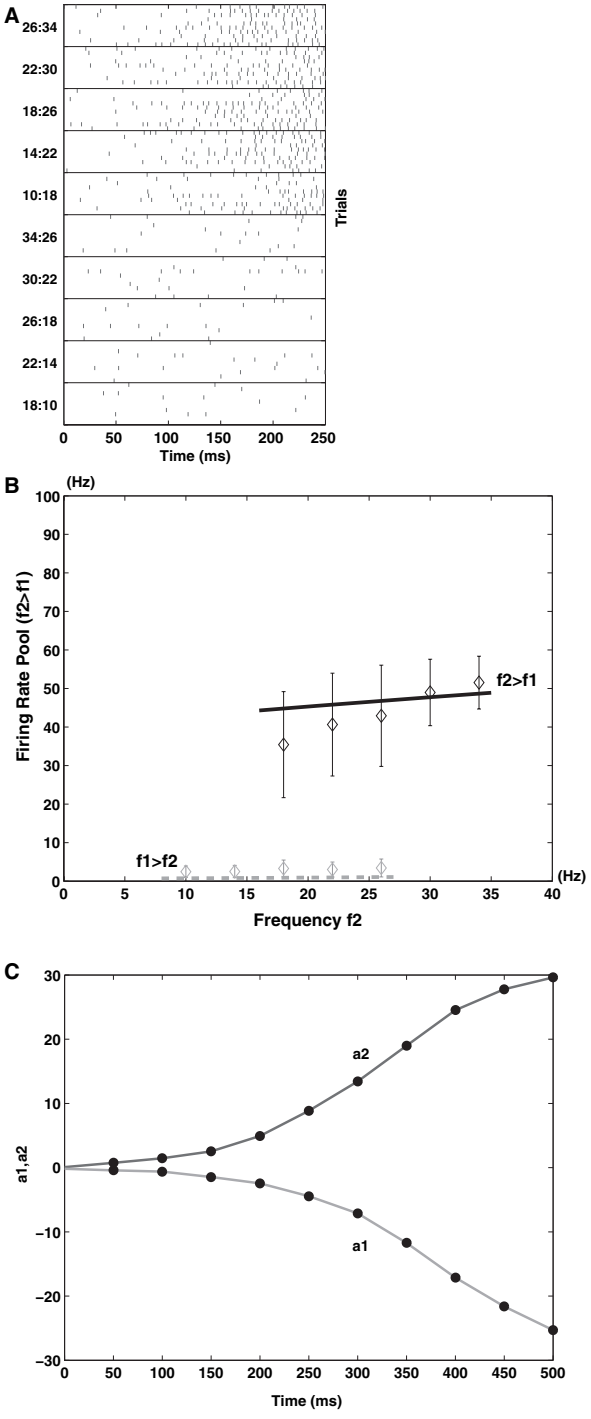

FIG. 7. Responses of a neuron of the population ($f_1 < f_2$) during the comparison period of f_1 and f_2 stimulation. The simulations corresponds to the experimental cases measured and studied by Romo *et al*. (2004) (see Fig. 2G–I of that paper). The different stimulation cases labelled on the left indicate f_1, f_2 pairs of vibrotactile stimulation frequencies. (A) Rastergrams. Each row of ticks is a trial, and each tick is a spike. All neurons were tested with ten trials for each stimulus pair, selecting only trials where the network performed correctly. (B) The average firing rate as a function of f_1 and f_2. The plots show the results obtained with the spiking simulations (diamond-points). The lines correspond to the mean-field calculations. The black indicates $f_1 < f_2$ ($f_2 = f_1 + 8$ Hz) and grey $f_1 > f_2$ ($f_2 = f_1 - 8$ Hz). (C) Evolution of fitting coefficients (see text) $a_1(t)$ and $a_2(t)$ during the comparison period. Both coefficients evolve in an antisymmetrical fashion, indicating that the average firing rate $r(t)$ is dependent only on the sign of the difference between f_1 and f_2 [i.e. $a_1(t) = -a_2(t)$], and not on the magnitude of the difference.

and by the absolute value of the frequency. This prediction could be tested by a trial-by-trial analysis of the neurophysiological data.

A second prediction is reflected in Fig. 8. We calculated for a fixed $f_2 = 25$ Hz and different $f_1 > f_2$ (from 1 Hz to 13 Hz), the probability of correct or incorrect discrimination, and the corresponding reaction time. The reaction time was the time that the winning population [($f_1 > f_2$) for the correct cases, and ($f_1 < f_2$) for the incorrect cases] took to cross a threshold of a firing rate of 20 Hz. (We averaged the reaction time over 200 trials). Figure 8A plots the relation between the reaction time and the probability of correct classification. The larger the probability of correct classification, the faster is the decision-making, which is reasonable and consistent with the decision-making literature. Figure 8B plots the reaction time of an incorrect decision, as a function of the probability of performing a misclassification. The behaviour is now the converse, in that a low probability of incorrect discrimination implies also shorter reaction times. This means that the reaction time of a correct or incorrect classification is similar, and therefore the dependence on the probability of a correct or incorrect classification is inverted.

The model also gives further insights into the mechanisms by which Weber's Law is implemented. We hypothesized that because $\Delta f/f$ is practically constant in the model, the difference of frequencies Δf required to push the single attractor network towards an attractor basin might increase with f because as f increases, shunting (divisive) inhibition produced by inhibitory feedback inputs (from the inhibitory interneurons) might act divisively on the pyramidal cell to shunt the excitatory inputs f_1 and f_2. In more detail, as the base frequency f increases, more excitation will be provided to the network by the inputs λ_1 and λ_2, this will tend to increase the firing rates of the pyramidal cells, which will in turn provide a larger excitatory input to the inhibitory neurons. This will tend to make the inhibitory neurons fire faster, and their GABA synapses onto the pyramidal cells will be more active. Because these GABA synapses open chloride channels and act with a driving potential $V_I = -70$ mV which is relatively close to the membrane potential (which will be in the range $V_L = -70$ mV to $V_{thr} = -50$ mV), a large part of the GABA synaptic input to the pyramidal cells will tend to shunt, that is to act divisively upon, the excitatory inputs to the pyramidal cells from the vibrotactile biasing inputs λ_1 and λ_2. To compensate for this current shunting effect, f_1 and f_2 are likely to need to increase in proportion to the base frequency f in order to maintain the efficacy of their biasing effect. To assess this hypothesis, we measured the change in conductance produced by the GABA inputs as a function of the base frequency, and show in Fig. 9 that the conductance increases linearly with the base frequency (as does the firing rate of the GABA neurons). The shunting effect does appear therefore to be dividing the excitatory inputs to the pyramidal cells in the linear way as a function of f that we hypothesized. We therefore propose that Weber's Law is implemented by shunting effects acting on pyramidal cells that are produced by inhibitory neuron inputs, which increase linearly as the base frequency increases, so that the difference of frequencies Δf

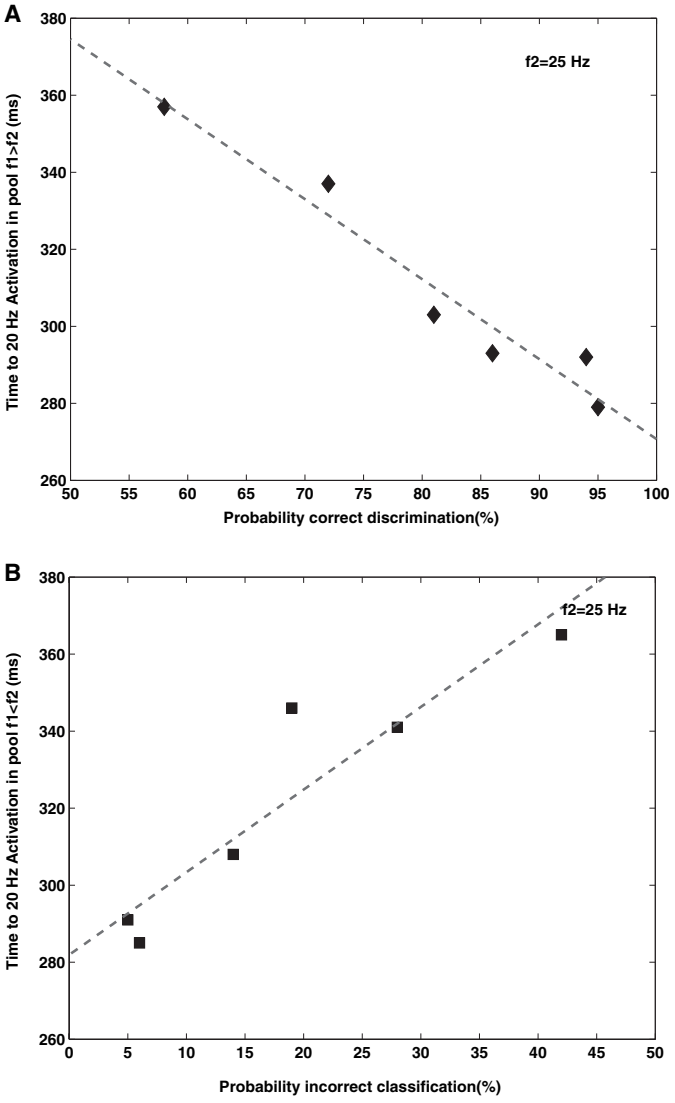

FIG. 8. Reaction time and probability dependence for a fixed $f_2 = 25$ Hz and different $f_1 > f_2$ (from 1 Hz to 13 Hz). The reaction time was the time that the winning population [($f_1 > f_2$) for the correct cases, and ($f_1 < f_2$) for the incorrect cases] took to cross a threshold of 20 Hz. (The reaction time was averaged across 200 trials.) (A) Reaction time as a function of the probability of correct classification. The larger the probability the faster is the decision-making. (B) Reaction time of an incorrect decision, as a function of the probability of performing a misclassification.

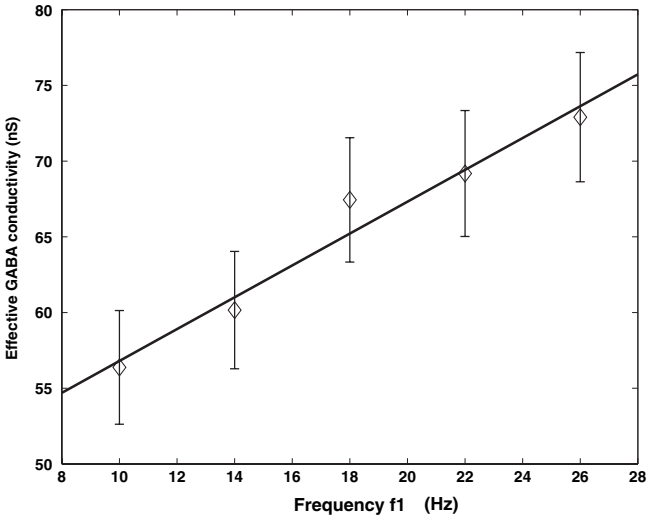

FIG. 9. The conductance in nS (mean ± SD) produced by the GABA inputs to the pyramidal cells as a function of the base frequency f_1. The effective conductance produced through the GABA synapses [i.e. $I_{GABA}/(V - V_I)$] was averaged over the time window in which the stimuli were presented in one of the excitatory neuron pools, when the base frequency was f_1 and $f_2 - f_1$ was set to 8 Hz.

required to push the network reliably into one of its attractors must increase in proportion to the base frequency. We checked the excitatory inputs to the pyramidal cells (for which $V_E = 0$ mV), and found that their conductances were much smaller (in the order of 5 nS for the AMPA and 15 nS for the NMDA receptors) than those produced by the GABA receptors, so that it is the GABA-induced conductance changes that dominate, and that produce the shunting inhibition.

The results described above indicate that the probabilistic settling of the system is related to the finite size noise effects of the spiking dynamics of the individual neurons with their Poisson-like spike trains in a system of limited size. To investigate this further, we simulated networks with different numbers of neurons, N. The noise due to the finite size effects is expected to increase as the network becomes smaller, and indeed to be proportional to $1/\sqrt{N}$. We show in Fig. 10 the effects of altering N on the operation of the network, where $N = N_E + N_I$, and $N_E : N_I$, was held at 4 : 1 as in the simulations shown earlier. The simulations were for $f_1 = 30$ Hz and $f_2 = 22$ Hz. Figure 10 shows overall that when N is larger than approximately 1000, the network shows the expected settling to the ($f_1 > f_2$) attractor state on a proportion of occasions that is in the range 85–93%, increasing only a little as the number of neurons reaches 4000 (top panel). The settling remains probabilistic, as shown by the standard deviations in the probability that the ($f_1 > f_2$) attractor state will be reached (top panel). When N is less than approximately 1000, the finite size noise effects become very marked, as shown by the fact that the network reaches the correct attractor state ($f_1 > f_2$) much less frequently, and in that the time for a decision to be reached can be premature and fast, as the large fluctuations in the stochastic noise can

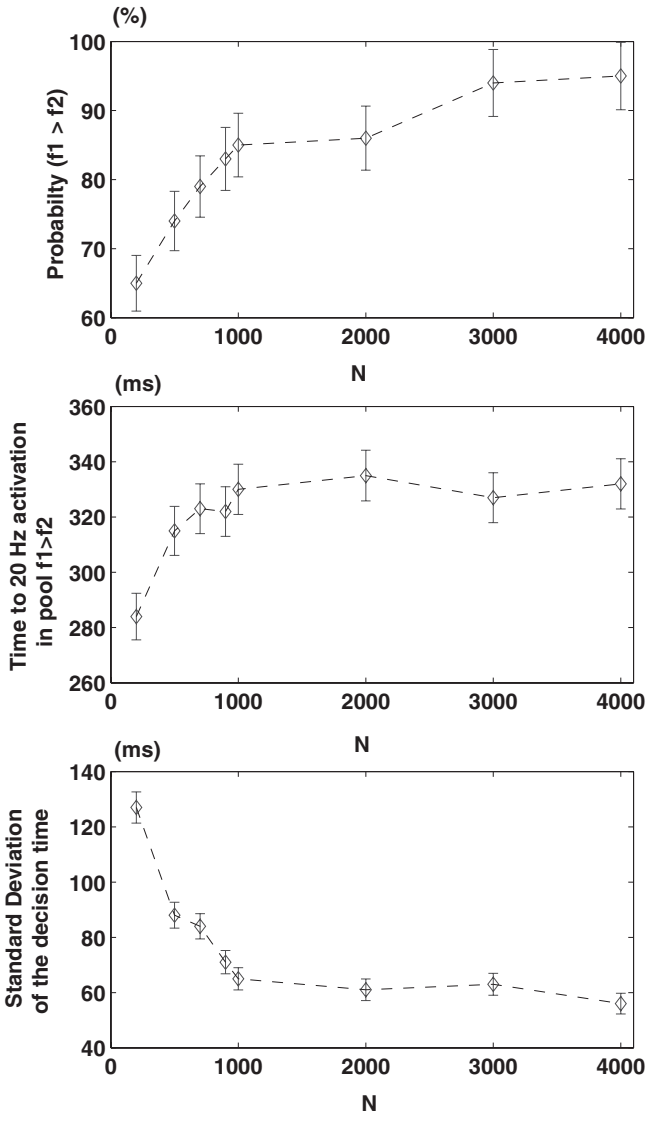

FIG. 10. The effects of altering N, the number of neurons in the network, on the operation of the network. The simulations were for $f_1 = 30$ Hz and $f_2 = 22$ Hz. The top panel shows the probability that the network will settle into the correct ($f_1 > f_2$) attractor state. The middle panel shows the time for a decision to be reached, that is for the system to reach a criterion of a firing rate of 20 Hz in the pool ($f_1 > f_2$). The bottom panel shows the standard deviation of the decision time.

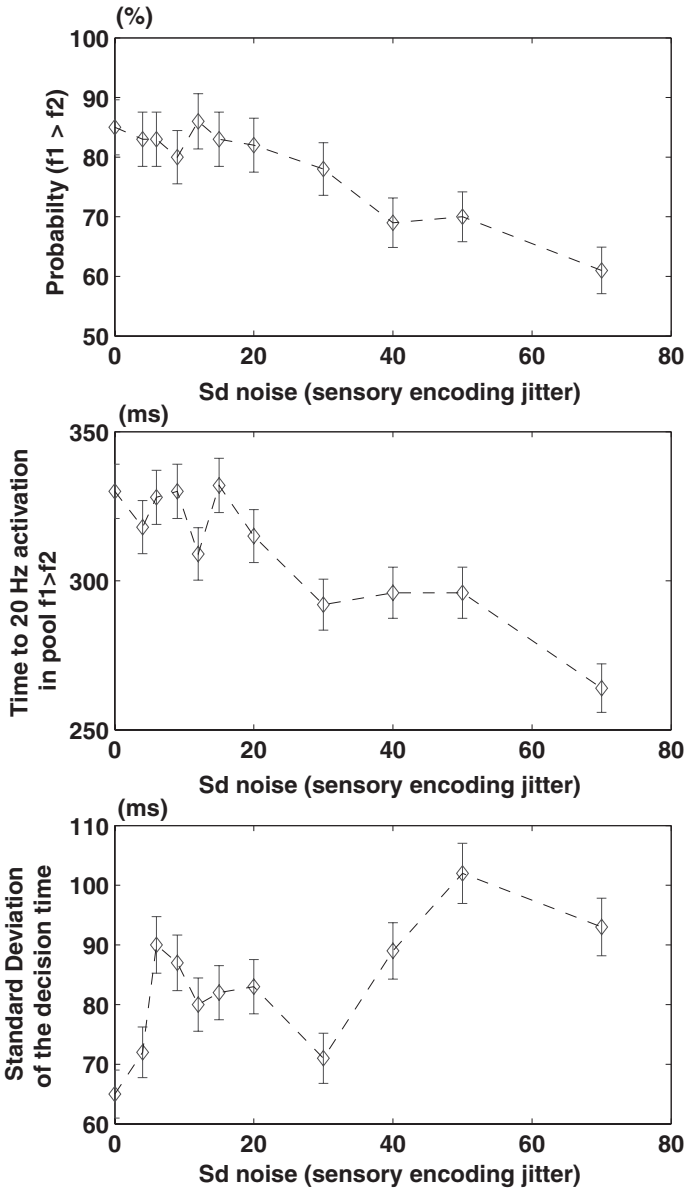

FIG. 11. The effects of adding noise to the inputs λ_1 and λ_2 to the network. The abscissa is the standard deviation of the noise added to λ_1 and λ_2, and $f_1 = 30$ Hz and $f_2 = 22$ Hz so that λ_1 was 85.8 Hz and λ_2 was 62.6 Hz. The top panel shows the probability that the network will settle into the correct ($f_1 > f_2$) attractor state. The middle panel shows the time for a decision to be reached, that is for the system to reach a criterion of a firing rate of 20 Hz in the pool ($f_1 > f_2$). The bottom panel shows the standard deviation of the decision time.

cause the system to reach the criterion [in this case of a firing rate of 20 Hz in the pool ($f_1 > f_2$)] too fast. The overall conclusion of the results shown in Fig. 10 is that the size of the network, N, does influence the probabilistic settling of the network to the decision state. None of these probabilistic attractor and decision-related settling effects would of course be found in a mean field or purely rate simulation, without spiking activity. The size of N in the brain is likely to be greater than 1000 (and probably in the neocortex in the range 4000–12 000; Rolls & Deco, 2002).

To examine further the effect of the internal finite size noise in comparison to noise in the inputs to the network, we performed further simulations in which uniform noise was added to the inputs λ_1 and λ_2 to the network. The results are shown in Fig. 11 for the normal network simulated with $N = 1000$. The abscissa is the standard deviation of the noise added to λ_1 and λ_2, and as in Fig. 10, $f_1 = 30$ Hz and $f_2 = 22$ Hz. (For these values, λ_1 is 85.8 Hz and λ_2 is 62.6 Hz, so that the added noise in Fig. 11 is quite significant compared to the inherent noise due to the Poisson nature of the input spikes to the network.) The results in Fig. 11 show that the operation of the network is little affected by noise in the inputs in the range up to SD = 20 spikes/s, and that with more input noise added, the performance of the network gradually deteriorates, as shown in the top panel (the proportion of correct decisions), and the premature decisions that are reached (middle panel). The overall conclusion of the results shown in Fig. 11 is that the network is relatively robust with respect to variability in the input, which only started to degrade performance when the standard deviation of the input noise was large compared to the inherent variability of the input due to its Poisson nature.

Discussion

Key properties of this biased attractor model of decision-making are that the decisions are taken probabilistically because of the finite size noise due to spiking activity in the integrate-and-fire dynamical network (Wang, 2002), with the probability that a particular decision is made depending on the biasing inputs provided by the sensory stimuli f_1 and f_2. We showed that the relevant parameters for the decision to be made to a criterion of a given per cent correct about whether f_1 is different from f_2 by the network are found not to be the absolute value of f_1 or f_2, but the difference between them scaled by their absolute value. If the difference between the two stimuli at which they can be discriminated $\Delta f = f_1 - f_2$, then it is found that Δf increases linearly as a function of the base frequency f_2, which is Weber's Law. The results show that Weber's law does not depend on the final firing rates of neurons in the attractor, but instead reflects the nature of the probabilistic settling into a decision-related attractor, which depends on the statistical fluctuations in the network, the synaptic connectivity, and the difference between the bias input frequencies f_1 and f_2 scaled by the baseline input f_2. We note that Weber's law is usually formulated as $\Delta f/(f_0 + f) =$ a constant, where f_0 allows the bottom part of the curve to asymptote at f_0. In vision, f_0 is sometimes referred to as 'dark light'. The result is that there is a part of the curve where Δf is linearly related to f, and the curve of Δf vs. f need not go through the origin. This corresponds to the data shown in Fig. 4.

An analysis of the non-stationary evolution of the dynamics of the network model, performed by explicit full spiking simulations, shows that Weber's law is implemented in the probability of transition from the initial spontaneous firing state to one of the two possible attractor states. In this decision-making paradigm, the firing rates of neurons in the VPC encode the outcome of the comparison and therefore the decision and motor response, but not how strong the stimuli are, i.e. what Weber called 'sensation' (as described for example in a detection task by de Lafuente & Romo, 2005). The probability of obtaining a specific decision, i.e. of detecting a just noticeable difference, is encoded in the stochastic dynamics of the network. More specifically, the origin of the fluctuations that will drive the transitions towards particular decisions depends on the connectivity between the different populations, on the size of the populations, and on the Poisson-like spike trains of the individual neurons in the system. In other words, the neural code for the outcome of the decision is reflected in the high rate of one of the populations of neurons, but whether the rate of a particular population becomes high is probabilistic. This means that an essential part of how the decision process is reached is contained in the synapses, in the finite size of the network (see Fig. 10), and in the Poisson-like firing of individual neurons in the network.

The fluctuations in the network are due to the finite size noise, which approximates to the square root of the (firing rate/number of neurons in the population), see Mattia & Del Giudice (2002), as shown in Figs 10 and 11. This is the first time we know when the implementation of a psychophysical law is not the firing rate of the neurons, nor the spike timing, nor is single neuron based, but instead is based on the synaptic connectivity of the network and on statistical fluctuations due to the spiking activity in the network.

The way in which the system settles (i.e. the probability of reaching one attractor state vs. the other from the initial spontaneous state, and the time it takes) depends on factors that include the distortion of the attractor landscapes produced by the biasing inputs λ_1 and λ_2, which will influence both the shapes and the depth of the attractor basins, and the finite size noise effects. Of particular importance in relation to Weber's law is likely to be that when λ_1 and λ_2 increase, the increased firing of the neurons in the two attractors results in more activity of the inhibitory feedback neurons, which then produce effectively divisive inhibition on the principal cells of the attractor network. This is reflected in the conductance change produced by the GABA inputs to the pyramidal cells shown in Fig. 9. The inhibitory feedback is mainly divisive because the GABA activated channels operate primarily as a current shunt, and do not produce much hyperpolarization, given that V_I is relatively close to the membrane potential. After the division implemented by the feedback inhibition, the differential bias required to push the network reliably into one of the attractors must then be larger, and effectively the driving force ($\lambda_1 - \lambda_2$ or $\Delta\lambda$) must get larger in proportion to the inhibition. As the inhibition is proportional to λ, this produces the result that $\Delta\lambda/\lambda$ is approximately a constant. We thus propose that Weber's Law, $\Delta I/I$ is a constant, is implemented by shunting effects acting on pyramidal cells that are produced by inhibitory neuron inputs which increase linearly as the baseline input I increases, so that the difference of intensities ΔI required to push the network reliably into one of its attractors must increase in proportion to the base input I. We emphasize that this account of Weber's Law is intended to be a general account, and is not restricted to the particular dataset or brain system against which the development of the model described here was validated. However, the results were obtained in a case where the sensory input neuronal firing is a linear function of stimulus frequency, as is the case for vibrotactile flutter sensory information (Romo *et al*., 2004), and it will be of interest to consider cases where the neuronal firing is a different, for example logarithmic, function of the input stimulus characteristics.

Another interesting aspect of the model is that the recurrent connectivity, and the relatively long time constant of the NMDA receptors (Wang, 2002), together enable the system to accumulate evidence over a long time period. For this reason, and to facilitate stability in the network, in the model there are NMDA receptors in the recurrent collateral connections. (Because NMDA receptors are not crucial to how the inputs produce their effects, they were not included

here in the interests of a minimal model to account for the neuronal data related to decision-making. For the same reason, point integrate-and-fire neurons were used rather than a more complicated multiple compartment model. Spiking neurons are of course essential to capture the probabilistic dynamics of the system.)

Although the model described here is effectively a single attractor network, we note that the network need not be localized to one brain region. Long-range connections between cortical areas enable networks in different brain areas to interact in the way needed to implement a single attractor network. The requirement is that the synapses between the neurons in any one pool be set up by Hebb-like associative synaptic modification, and this is likely to be a property of connectivity between areas as well as within areas (Rolls & Treves, 1998; Rolls & Deco, 2002). In this sense, the decision could be thought of as distributed across different brain areas. Consistent with this, Romo and colleagues have found neurons related to vibrotactile decisions not only in VPC, but in a number of connected brain areas including MPC (see Materials and methods). In order to achieve the desired probabilistic settling behaviour, the network we describe must not have very high inhibition, and, related to this, may sometimes not settle into one of its attractor states. In a forced choice task in which a decision must be reached on every trial, a possible solution is to have a second decision-making network, with parameters adjusted so that it will settle into one of its states (chosen at chance) even if a preceding network in the decision-making chain has not settled. This could be an additional reason for having a series of networks in different brain regions involved in the decision-making process.

The model described here is different in a number of ways from accumulator or counter models, which may include a noise term and which undergo a random walk in real time, which is a diffusion process [Carpenter & Williams, 1995; Ratcliff *et al*., 1999; see further Wang (2002) and Usher & McClelland (2001)]. In accumulator models, a mechanism for computing the difference between the stimuli is not described, whereas in the current model this is achieved, and scaled by f, by the feedback inhibition included in the attractor network. Second, in the current model the decision corresponds to high firing rates in one of the attractors, and there is no arbitrary threshold that must be reached. Third, the noise in the current model is not arbitrary, but is accounted for by finite size noise effects of the spiking dynamics of the individual neurons with their Poisson-like spike trains in a system of limited size. Fourth, because the attractor network has recurrent connections, the way in which it settles into a final attractor state (and thus the decision process) can naturally take place over quite a long time, as information gradually and stochastically builds up due to the positive feedback in the recurrent network, the weights in the network, and the biasing inputs, as shown in Figs 6 and 7.

The current model of decision-making is part of a unified approach to attention, reward-reversal, and sequence learning, in which biasing inputs influence the operation of attractor networks that operate using biased competition (Rolls & Deco, 2002; Deco & Rolls, 2005a; Rolls, 2005). The same approach is now seen to be useful in understanding the neuronal activity underlying decision-making and its relation to Weber's Law.

The model makes specific neurophysiological predictions. One, on reaction times in relation to $\Delta f/f$, is shown in Fig. 8. Another prediction is that the model shows that Weber's law for frequency discrimination could be implemented not by the firing rate of a given population of neurons (which reflects just the discrete decision taken), but by the probability that a particular population will be activated, which depends on $\Delta f/f$. This prediction could be tested by a trial-by-trial analysis of the neurophysiological data in which the firing of neurons at different base frequencies f and for different Δf is measured, to investigate whether the type of result shown in Fig. 3, and thereby in Fig. 4, which are derived from the model, are also found in the neuronal data from the experiments, and this would also usefully confirm that Weber's Law holds at the neuronal level in this particular vibrotactile task with a delay. In particular, although Romo *et al*. (2004) in their Fig. 5 show that choice probability and neuronal activity increases as a function of $f_2 - f_1$, we predict that neurons should follow the functions shown in Figs 3 and 4 for different values of Δf and f, and it would be of interest to test this prediction. We note that Weber's law holds in most though not all discrimination situations, and to the extent that Weber's law does generally hold, the model described here provides a computational neuroscience-based account of how it arises. This is the first time we know when the implementation of a psychophysical law is not the firing rate of the neurons, nor the spike timing, nor is single neuron based, but instead is based on the synaptic connectivity of the network and on statistical fluctuations due to the spiking activity in the network.

Acknowledgements

Gustavo Deco was supported by Institucion Catalana de recerca i Estudis Avanats (ICREA). The research was supported by the McDonnell Centre for Cognitive Neuroscience at the University of Oxford, and by the Medical Research Council. Dr R. Romo is thanked for helpful discussions. This work was supported by the European Union, grant EC005-024 (STREP "Decisions in Motion") and by the Spanish Research Project TIN2004-04363-C03-01.

Abbreviations

MPC, medial premotor cortex; PFC, prefrontal cortex; S1, primary somatosensory area; S2, secondary somatosensory area; VPC, ventral premotor cortex.

References

Abeles, M. (1991) *Corticonics – Neural Circuits of the Cerebral Cortex*. Cambridge University Press, New York.

Amit, D.J. & Brunel, N. (1997) Model of global spontaneous activity and local structured activity during delay periods in the cerebral cortex. *Cereb. Cortex*, **7**, 237–252.

Brody, C.D., Hernandez, A., Zainos, A., Lemus, L. & Romo, R. (2002) Analysing neuronal correlates of the comparison of two sequentially presented sensory stimuli. *Philos. Trans. R. Soc. Lond. B Biol. Sci.*, **357**, 1843–1850.

Brody, C.D., Hernandez, A., Zainos, A. & Romo, R. (2003a) Timing and neural encoding of somatosensory parametric working memory in macaque prefrontal cortex. *Cereb. Cortex*, **13**, 1196–1207.

Brody, C.D., Romo, R. & Kepecs, A. (2003b) Basic mechanisms for graded persistent activity: discrete attractors, continuous attractors, and dynamic representations. *Curr. Opin. Neurobiol.*, **13**, 204–211.

Brunel, N. & Wang, X.J. (2001) Effects of neuromodulation in a cortical network model of object working memory dominated by recurrent inhibition. *J. Comput. Neurosci.*, **11**, 63–85.

Carpenter, R.H.S. & Williams, M.L. (1995) Neural computation of log likelihood in control of saccadic eye movements. *Nature*, **377**, 59–62.

Corchs, S. & Deco, G. (2002) Large-scale neural model for visual attention: integration of experimental single-cell and fMRI data. *Cereb. Cortex*, **12**, 339–348.

Corchs, S. & Deco, G. (2004) Feature-based attention in human visual cortex: simulation of fMRI data. *Neuroimage*, **21**, 36–45.

Deco, G. & Lee, T.S. (2002) A unified model of spatial and object attention based on inter-cortical biased competition. *Neurocomputing*, **44–46**, 775–781.

Deco, G., Pollatos, O. & Zihl, J. (2002) The time course of selective visual attention: theory and experiments. *Vis. Res.*, **42**, 2925–2945.

Deco, G. & Rolls, E.T. (2002) Object-based visual neglect: a computational hypothesis. *Eur. J. Neurosci.*, **16**, 1994–2000.

Deco, G. & Rolls, E.T. (2003) Attention and working memory: a dynamical model of neuronal activity in the prefrontal cortex. *Eur. J. Neurosci.*, **18**, 2374–2390.

Deco, G. & Rolls, E.T. (2004) A neurodynamical cortical model of visual attention and invariant object recognition. *Vis. Res.*, **44**, 621–644.
Deco, G. & Rolls, E.T. (2005a) Attention, short-term memory, and action selection: a unifying theory. *Prog. Neurobiol.*, **76**, 236–256.
Deco, G. & Rolls, E.T. (2005b) Neurodynamics of biased competition and co-operation for attention: a model with spiking neurons. *J. Neurophysiol.*, **94**, 295–313.
Deco, G., Rolls, E.T. & Horwitz, B. (2004) 'What' and 'where' in visual working memory: a computational neurodynamical perspective for integrating fMRI and single-neuron data. *J. Cogn. Neurosci.*, **16**, 683–701.
Deco, G., Rolls, E.T. & Zihl, J. (2005) A neurodynamical model of visual attention. In Itti, L., Rees, G. & Tsotos, J., (Eds), *Neurobiology of Attention*. Elsevier, San Diego, CA, pp. 593–599.
Gold, J.I. & Shadlen, M.N. (2000) Representation of a perceptual decision in developing oculomotor commands. *Nature*, **404**, 390–394.
Hernandez, A., Zainos, A. & Romo, R. (2002) Temporal evolution of a decision-making process in medial premotor cortex. *Neuron*, **33**, 959–972.
Hestrin, S., Sah, P. & Nicoll, R.A. (1990) Mechanisms generating the time course of dual component excitatory synaptic currents recorded in hippocampal slices. *Neuron*, **5**, 247–253.
Jahr, C.E. & Stevens, C.F. (1990) Voltage dependence of NMDA-activated macroscopic conductances predicted by single-channel kinetics. *J. Neurosci.*, **10**, 3178–3182.
de Lafuente, V. & Romo, R. (2005) Neuronal correlates of subjective sensory experience. *Nature Neurosci.*, **12**, 1698–1703.
Machens, C.K., Romo, R. & Brody, C.D. (2005) Flexible control of mutual inhibition: a neural model of two-interval discrimination. *Science*, **307**, 1121–1124.
Mattia, M. & Del Giudice, P. (2002) Attention and working memory: a dynamical model of neuronal activity in the prefrontal cortex. *Phys. Rev. E*, **66**, 51917–51919.
McCormick, D.A., Connors, B.W., Lighthall, J.W. & Prince, D.A. (1985) Comparative electrophysiology of pyramidal and sparsely spiny stellate neurons of the neocortex. *J. Neurophysiol.*, **54**, 782–806.
Mountcastle, V.B., Steinmetz, M.A. & Romo, R. (1990) Frequency discrimination in the sense of flutter: psychophysical measurements correlated with postcentral events in behaving monkeys. *J. Neurosci.*, **10**, 3032–3044.
Ratcliff, R., Van Zandt, T. & McKoon, G. (1999) Connectionist and diffusion models of reaction time. *Psychol. Rev.*, **106**, 261–300.
Rolls, E.T. (2005) *Emotion Explained*. Oxford University Press, Oxford.
Rolls, E.T. & Deco, G. (2002) *Computational Neuroscience of Vision*. Oxford University Press, Oxford.
Rolls, E.T. & Treves, A. (1998) *Neural Networks and Brain Function*. Oxford University Press, Oxford.
Romo, R., Hernandez, A. & Zainos, A. (2004) Neuronal correlates of a perceptual decision in ventral premotor cortex. *Neuron*, **41**, 165–173.
Romo, R., Hernandez, A., Zainos, A., Lemus, L. & Brody, C.D. (2002) Neuronal correlates of decision-making in secondary somatosensory cortex. *Nature Neurosci.*, **5**, 1217–1225.
Romo, R., Hernandez, A., Zainos, A. & Salinas, E. (2003) Correlated neuronal discharges that increase coding efficiency during perceptual discrimination. *Neuron*, **38**, 649–657.
Romo, R. & Salinas, E. (2001) Touch and go: decision-making mechanisms in somatosensation. *Annu. Rev. Neurosci.*, **24**, 107–137.
Romo, R. & Salinas, E. (2003) Flutter discrimination: neural codes, perception, memory and decision making. *Nature Rev. Neurosci.*, **4**, 203–218.
Salin, P.A. & Prince, D.A. (1996) Spontaneous GABA-A receptor-mediated inhibitory currents in adult rat somatosensory cortex. *J. Neurophysiol.*, **75**, 1573–1588.
Spruston, N., Jonas, P. & Sakmann, B. (1995) Dendritic glutamate receptor channels in rat hippocampal CA3 and CA1 pyramidal neurons. *J. Physiol.*, **482**, 325–352.
Szabo, M., Almeida, R., Deco, G. & Stetter, M. (2004) Cooperation and biased competition model can explain attentional filtering in the prefrontal cortex. *Eur. J. Neurosci.*, **19**, 1969–1977.
Tuckwell, H. (1988) *Introduction to Theoretical Neurobiology.* Cambridge University Press, Cambridge.
Usher, M. & McClelland, J.L. (2001) The time course of perceptual choice: the leaky, competing accumulator model. *Psychol. Rev.*, **108**, 550–592.
Wang, X.J. (2002) Probabilistic decision making by slow reverberation in cortical circuits. *Neuron*, **36**, 955–968.
Xiang, Z., Huguenard, J.R. & Prince, D.A. (1998) GABA-A receptor-mediated currents in interneurons and pyramidal cells of rat visual cortex. *J. Physiol.*, **506**, 715–730.

Appendix 1

We used the mathematical formulation of integrate-and-fire (IF) neurons and synaptic currents described by Brunel & Wang (2001). Here we provide a brief summary of this framework, which we have extended to multiple interacting networks. The dynamics of the subthreshold membrane potential V of a neuron are given by the equation:

$$C_{\mathrm{m}}\frac{\mathrm{d}V(t)}{\mathrm{d}t} = -g_{\mathrm{m}}(V(t)-V_{\mathrm{L}}) - I_{\mathrm{syn}}(t)$$

where C_{m} is the membrane capacitance taken to be 0.5 nF for excitatory neurons and 0.2 nF for inhibitory neurons; g_{m} is the membrane leak conductance taken to be 25 nS for excitatory neurons and 20 nS for inhibitory neurons; V_{L} is the resting potential of −70 mV and I_{syn} is the synaptic current. The firing threshold is taken to be $V_{\mathrm{thr}} = -50$ mV and the reset potential $V_{\mathrm{reset}} = -55$ mV (see McCormick *et al.*, 1985).

The synaptic current is given by a sum of glutamatergic, AMPA ($I_{\mathrm{AMPA,rec}}$) and NMDA ($I_{\mathrm{NMDA,rec}}$) mediated, recurrent excitatory currents, one AMPA ($I_{\mathrm{AMPA,ext}}$) mediated external excitatory current and one inhibitory GABAergic current (I_{GABA}):

$$I_{\mathrm{syn}}(t) = I_{\mathrm{AMPA,ext}}(t) + I_{\mathrm{AMPA,rec}}(t) + I_{\mathrm{NMDA,rec}}(t) + I_{\mathrm{GABA}}(t)$$

The currents are defined by:

$$I_{\mathrm{AMPA,ext}}(t) = g_{\mathrm{AMPA,ext}}(V(t)-V_{\mathrm{E}})\sum_{j=1}^{N_{\mathrm{ext}}} s_j^{\mathrm{AMPA,ext}}(t)$$

$$I_{\mathrm{AMPA,rec}}(t) = g_{\mathrm{AMPA,rec}}(V(t)-V_{\mathrm{E}})\sum_{j=1}^{N_{\mathrm{E}}} w_j s_j^{\mathrm{AMPA,rec}}(t)$$

$$I_{\mathrm{NMDA,rec}}(t) = \frac{g_{\mathrm{NMDA,rec}}(V(t)-V_{\mathrm{E}})}{1+[\mathrm{Mg}^{++}]\exp(-0.062\,V(t))/3.57}\times\sum_{j=1}^{N_{\mathrm{E}}} w_j s_j^{\mathrm{NMDA,rec}}(t)$$

$$I_{\mathrm{GABA}}(t) = g_{\mathrm{GABA}}(V(t)-V_{\mathrm{I}})\sum_{j=1}^{N_{\mathrm{I}}} s_j^{\mathrm{GABA}}(t)$$

where $V_{\mathrm{E}} = 0$ mV, $V_{\mathrm{I}} = -70$ mV, w_j are the synaptic weights, each receptor has its own fraction s_j of open channels, and its own synaptic conductance g. The NMDA synaptic current is dependent on the potential and controlled by the extracellular concentration of magnesium ($[\mathrm{Mg}^{++}] = 1$ mM) (Jahr & Stevens, 1990). The values for the synaptic conductances for excitatory neurons are $g_{\mathrm{AMPA,ext}} = 2.08$ nS, $g_{\mathrm{AMPA,rec}} = 0.104$ nS, $g_{\mathrm{NMDA}} = 0.327$ nS and $g_{\mathrm{GABA}} = 1.287$ nS; and for inhibitory neurons $g_{\mathrm{AMPA,ext}} = 1.62$ nS, $g_{\mathrm{AMPA,rec}} = 0.081$ nS, $g_{\mathrm{NMDA}} = 0.258$ nS and $g_{\mathrm{GABA}} = 1.002$ nS. These values are obtained from the ones used in Brunel & Wang (2001) by multiplication by a factor, which corrects for the difference in number of neurons used in our and Brunel and Wang's model. In their work the conductances were calculated so that in an unstructured network the excitatory neurons have a spontaneous spiking rate of 3 Hz and the inhibitory neurons a spontaneous rate of 9 Hz.

The fractions of open channels are described by:

$$\frac{\mathrm{d}s_j^{\mathrm{AMPA,ext}}(t)}{\mathrm{d}t} = -\frac{s_j^{\mathrm{AMPA,ext}}(t)}{\tau_{\mathrm{AMPA}}} + \sum_k \delta(t-t_j^k)$$

$$\frac{\mathrm{d}s_j^{\mathrm{AMPA,rec}}(t)}{\mathrm{d}t} = -\frac{s_j^{\mathrm{AMPA,rec}}(t)}{\tau_{\mathrm{AMPA}}} + \sum_k \delta(t - t_j^k)$$

$$\frac{\mathrm{d}s_j^{\mathrm{NMDA}}(t)}{\mathrm{d}t} = -\frac{s_j^{\mathrm{NMDA}}(t)}{\tau_{\mathrm{NMDA,decay}}} + \alpha x_j(t)(1 - s_j^{\mathrm{NMDA}}(t))$$

$$\frac{\mathrm{d}x_j(t)}{\mathrm{d}t} = -\frac{x_j(t)}{\tau_{\mathrm{NMDA,rise}}} + \sum_k \delta(t - t_j^k)$$

$$\frac{\mathrm{d}s_j^{\mathrm{GABA}}(t)}{\mathrm{d}t} = -\frac{s_j^{\mathrm{GABA}}(t)}{\tau_{\mathrm{GABA}}} + \sum_k \delta(t - t_j^k),$$

where the rise time constant for NMDA synapses is $\tau_{\mathrm{NMDA,rise}} = 2$ ms (Hestrin *et al*., 1990; Spruston *et al*., 1995), the rise time constants for AMPA and GABA are neglected because they are smaller than 1 ms, and $\alpha = 0.5$ m/s. All synapses have a delay of 0.5 ms. The decay time constant for the AMPA synapses is $\tau_{\mathrm{AMPA}} = 2$ ms (Hestrin *et al*., 1990; Spruston *et al*., 1995), for NMDA synapses is $\tau_{\mathrm{NMDA,decay}} = 100$ ms (Hestrin *et al*., 1990; Spruston *et al*., 1995), and for GABA synapses $\tau_{\mathrm{GABA}} = 10$ ms (Salin & Prince, 1996; Xiang *et al*., 1998). The sums over k represent a sum over spikes formulated as δ-Peaks [$\delta(t)$] emitted by presynaptic neuron j at time t_j^k.

Appendix 2

The mean-field approximation used in the present work was derived by Brunel & Wang (2001), assuming that the network of integrate-and-fire neurons is in a stationary state. In this formulation the potential of a neuron is calculated as:

$$\tau_x \frac{\mathrm{d}V(t)}{\mathrm{d}t} = -V(t) + \mu_x + \sigma_x \sqrt{\tau_x}\eta(t)$$

where $V(t)$ is the membrane potential, x labels the populations, τ_x is the effective membrane time constant, μ_x is the mean value the membrane potential would have in the absence of spiking and fluctuations, σ_x measures the magnitude of the fluctuations and η is a Gaussian process with absolute exponentially decaying correlation function with time constant τ_{AMPA}. The quantities μ_x and ${\sigma_x}^2$ are given by:

$$\mu_x = [(T_{\mathrm{ext}} v_{\mathrm{ext}} + T_{\mathrm{AMPA}} n_x^{\mathrm{AMPA}} + \rho_1 n_x^{\mathrm{NMDA}}) V_{\mathrm{E}} + \rho_2 n_x^{\mathrm{NMDA}} \langle V \rangle + T_{\mathrm{I}} n_x^{\mathrm{GABA}} V_{\mathrm{I}} + V_{\mathrm{L}}]/S_x \quad (1)$$

$$\sigma_x^2 = \frac{g_{\mathrm{AMPA,ext}}^2 (\langle V \rangle - V_{\mathrm{E}})^2 N_{\mathrm{ext}} v_{\mathrm{ext}} \tau_{\mathrm{AMPA}}^2 \tau_x}{g_{\mathrm{m}}^2 \tau_{\mathrm{m}}^2} \quad (2)$$

where v_{ext} Hz is the external incoming spiking rate, v_{I} is the spiking rate of the inhibitory population, $\tau_{\mathrm{m}} = C_{\mathrm{m}}/g_{\mathrm{m}}$ with the values for the excitatory or inhibitory neurons depending of the population considered and the other quantities are given by:

$$S_x = 1 + T_{\mathrm{ext}} v_{\mathrm{ext}} + T_{\mathrm{AMPA}} n_x^{\mathrm{AMPA}} + (\rho_1 + \rho_2) n_x^{\mathrm{NMDA}} + T_{\mathrm{I}} n_x^{\mathrm{GABA}} \quad (3)$$

$$\tau_x = \frac{C_{\mathrm{m}}}{g_{\mathrm{m}} S_x} \quad (4)$$

$$n_x^{\mathrm{AMPA}} = \sum_{j=1}^{p} r_j w_{jx}^{\mathrm{AMPA}} v_j \quad (5)$$

$$n_x^{\mathrm{NMDA}} = \sum_{j=1}^{p} r_j w_{jx}^{\mathrm{NMDA}} \psi(v_j) \quad (6)$$

$$n_x^{\mathrm{GABA}} = \sum_{j=1}^{p} r_j w_{jx}^{\mathrm{GABA}} v_j \quad (7)$$

$$\psi(v) = \frac{v\tau_{\mathrm{NMDA}}}{1 + v\tau_{\mathrm{NMDA}}} \left(1 + \frac{1}{1 + v\tau_{\mathrm{NMDA}}} \sum_{n=1}^{\infty} \frac{(-\alpha\tau_{\mathrm{NMDA,rise}})^n T_n(v)}{(n+1)!}\right) \quad (8)$$

$$T_n(v) = \sum_{k=0}^{n} (-1)^k \binom{n}{k} \frac{\tau_{\mathrm{NMDA,rise}}(1 + v\tau_{\mathrm{NMDA}})}{\tau_{\mathrm{NMDA,rise}}(1 + v\tau_{\mathrm{NMDA}}) + k\tau_{\mathrm{NMDA,decay}}} \quad (9)$$

$$\tau_{\mathrm{NMDA}} = \alpha\tau_{\mathrm{NMDA,rise}}\tau_{\mathrm{NMDA,decay}} \quad (10)$$

$$T_{\mathrm{ext}} = \frac{g_{\mathrm{AMPA,ext}}\tau_{\mathrm{AMPA}}}{g_{\mathrm{m}}} \quad (11)$$

$$T_{\mathrm{AMPA}} = \frac{g_{\mathrm{AMPA,rec}} N_{\mathrm{E}} \tau_{\mathrm{AMPA}}}{g_{\mathrm{m}}} \quad (12)$$

$$\rho_1 = \frac{g_{\mathrm{NMDA}} N_{\mathrm{E}}}{g_{\mathrm{m}} J} \quad (13)$$

$$\rho_2 = \beta \frac{g_{\mathrm{NMDA}} N_{\mathrm{E}} (\langle V_x \rangle - V_{\mathrm{E}})(J - 1)}{g_{\mathrm{m}} J^2} \quad (14)$$

$$J = 1 + \gamma \exp(-\beta \langle V_x \rangle) \quad (15)$$

$$T_{\mathrm{I}} = \frac{g_{\mathrm{GABA}} N_{\mathrm{I}} \tau_{GABA}}{g_{\mathrm{m}}} \quad (16)$$

$$\langle V_x \rangle = \mu_x - (V_{\mathrm{thr}} - V_{\mathrm{reset}}) v_x \tau_x, \quad (17)$$

where p is the number of excitatory populations, r_x is the fraction of neurons in the excitatory x population, w_{jx} the weight of the connections from population x to population j, v_x is the spiking rate of the x excitatory population, $\gamma = [\mathrm{Mg}^{++}]/3.57$, $\beta = 0.062$ and the average membrane potential $\langle Vx \rangle$ has a value between −55 mV and 50 mV.

The spiking rate of a population as a function of the defined quantities is then given by:

$$v_x = \phi(\mu_x, \sigma_x), \quad \text{where} \quad (18)$$

$$\phi(\mu_x, \sigma_x) = \left(\tau_{\mathrm{rp}} + \tau_x \int_{\beta(\mu_x,\sigma_x)}^{\alpha(\mu_x,\sigma_x)} \mathrm{d}u \sqrt{\pi} \exp(u^2)[1 + \mathrm{erf}(u)]\right)^{-1} \quad (19)$$

$$\alpha(\mu_x, \sigma_x) = \frac{(V_{\mathrm{thr}} - \mu_x)}{\sigma_x} \left(1 + 0.5\frac{\tau_{\mathrm{AMPA}}}{\tau_x}\right) + 1.03\sqrt{\frac{\tau_{\mathrm{AMPA}}}{\tau_x}} - 0.5\frac{\tau_{\mathrm{AMPA}}}{\tau_x} \quad (20)$$

$$\beta(\mu_x, \sigma_x) = \frac{(V_{\text{reset}} - \mu_x)}{\sigma_x} \tag{21}$$

with erf(u) the error function and τ_{rp} the refractory period, which is considered to be 2 ms for excitatory neurons and 1 ms for inhibitory neurons. To solve the equations defined by Eqn 18 for all xs we numerically integrate Eqn 17 and the differential equation below, which has fixed point solutions corresponding to Eqn 18:

$$\tau_x \frac{\mathrm{d}v_x}{\mathrm{d}t} = -v_x + \phi(\mu_x, \sigma_x) \tag{22}$$

Appendix 3

In this appendix we bring together the fixed parameters of the model in Table 1, and then provide information about the values of further parameters used in the simulations, and how well the simulations fit the experimental data.

TABLE 1. Parameters used in the integrate-and-fire simulations

N_{E}	800
N_{I}	200
r	0.1
w_+	2.2
w_{I}	1.015
N_{ext}	800
ν_{ext}	2.4 kHz
C_{m} (excitatory)	0.5 nF
C_{m} (inhibitory)	0.2 nF
g_{m} (excitatory)	25 nS
g_{m} (inhibitory)	20 nS
V_{L}	−70 mV
V_{thr}	−50 mV
V_{reset}	−55 mV
V_{E}	0 mV
V_{I}	−70 mV
$g_{\text{AMPA,ext}}$ (excitatory)	2.08 nS
$g_{\text{AMPA,rec}}$ (excitatory)	0.104 nS
g_{NMDA} (excitatory)	0.327 nS
g_{GABA} (excitatory)	1.25 nS
$g_{\text{AMPA,ext}}$ (inhibitory)	1.62 nS
$g_{\text{AMPA,rec}}$ (inhibitory)	0.081 nS
g_{NMDA} (inhibitory)	0.258 nS
g_{GABA} (inhibitory)	0.973 nS
$\tau_{\text{NMDA,decay}}$	100 ms
$\tau_{\text{NMDA,rise}}$	2 ms
τ_{AMPA}	2 ms
τ_{GABA}	10 ms
α	0.5 m/s